ELSEVIER

Journal of Alloys and Compounds 446–447 (2007) 345–349

Journal of ALLOYS AND COMPOUNDS

www.elsevier.com/locate/jallcom

Hydrogen storage properties of $2LiNH_2 + LiBH_4 + MgH_2$

Jun Yang [a,*], Andrea Sudik [a], Donald J. Siegel [a], Devin Halliday [a], Andy Drews [a], Roscoe O. Carter III [a], Christopher Wolverton [a], Gregory J. Lewis [b], J.W.A. Sachtler [b], John J. Low [b], Syed A. Faheem [b], David A. Lesch [b], Vidvuds Ozolins [c]

[a] *Ford Motor Company, Research and Advanced Engineering, MD 1170/RIC, Dearborn, MI 48121, USA*
[b] *UOP LLC, 25 East Algonquin Road, Des Plaines, IL 60017-5017, USA*
[c] *Department of Materials Science and Engineering, University of California, Los Angeles, CA 90095-1595, USA*

Received 27 October 2006; received in revised form 21 March 2007; accepted 22 March 2007
Available online 5 April 2007

Abstract

We have investigated the ternary mixture of complex hydrides with stoichiometry $2LiNH_2 + LiBH_4 + MgH_2$, and have identified a set of novel hydrogen storage reactions. One of these reactions involves the known reversible reaction $Mg(NH_2)_2 + 2LiH \leftrightarrow Li_2Mg(NH)_2 + 2H_2$. Previous studies have shown that initiating this reaction from the binary mixture $2LiNH_2 + MgH_2$ results in poor hydrogen desorption kinetics and a small amount of NH_3 release. In contrast to this behavior, here we demonstrate that by starting from the *ternary* mixture $2LiNH_2 + LiBH_4 + MgH_2$, the above reaction can proceed at lower temperatures *and* with improved kinetics, while maintaining reversibility. The advantage of starting with the ternary mixture can be traced to the subsequent formation, melting, and reaction of $Li_4BH_4(NH_2)_3$ with MgH_2 to form the mixed imide phase $Li_2Mg(NH)_2$, which acts as a seed for the reversible reaction, and is at least partly responsible for the improved kinetic response.

Keywords: $Li_2Mg(NH)_2$; $LiNH_2$; $LiBH_4$; MgH_2; Hydrogen storage; Self-catalyzing

1. Introduction

Complex hydrides such as $NaAlH_4$, $LiNH_2$ and $LiBH_4$ are promising candidates for reversible solid-state hydrogen storage applications due to their high hydrogen densities. However, in their pure form the practical utility of most of these hydrides are limited by slow kinetics, irreversibility, and/or high desorption temperatures. Recently, it has been recognized that a viable strategy for overcoming these limitations involves combining complex hydrides with small amounts of a catalytic dopant or via reactions with other compounds [1–3]. In regards to the later strategy, the reversible reaction involving amides and imides of lithium and magnesium,

$$Mg(NH_2)_2 + 2LiH \leftrightarrow Li_2Mg(NH)_2 + 2H_2 \quad (1)$$

has been found to have desirable thermodynamics for release and reabsorption of hydrogen at moderate temperatures and pressures [4,5]. However, the observed reaction kinetics of this reaction is inhibited, requiring temperatures of 220 °C or more for reasonable rates of hydrogen release. Additionally, a small amount of NH_3 accompanies the release of H_2, an undesirable attribute as NH_3 can poison PEM fuel cells. In this paper, we will describe a novel scheme that results in significantly enhanced desorption kinetics for reaction (1) at lower temperatures while suppressing NH_3 release. These improved properties were identified in the course of exploring the ternary composition, $2LiNH_2 + LiBH_4 + MgH_2$.

2. Experimental

Lithium amide ($LiNH_2$) (95% purity, Sigma–Aldrich), magnesium hydride (MgH_2) (95% purity, Gelest) and lithium borohydride ($LiBH_4$) (95% purity, Sigma–Aldrich) were used as received. All sample handling was performed in an MBraun Labmaster 130 glovebox maintained under argon atmosphere with

* Corresponding author. Tel.: +1 313 337 9803.
E-mail address: jyang27@ford.com (J. Yang).

0925-8388/$ – see front matter © 2007 Elsevier B.V. All rights reserved.
doi:10.1016/j.jallcom.2007.03.145

<0.1 ppm O_2 and H_2O vapor. Two grams of a mixture of $LiNH_2$, $LiBH_4$ and MgH_2 in a 2:1:1 molar ratio mixture was loaded into a milling vial containing three stainless steel balls weighing 8.4 g each. Mechanical milling was carried out using a Spex 8000 mixer/mill for 1–20 h.

Variable temperature hydrogen desorption and gas composition were monitored using a temperature-programmed desorption (TPD) apparatus constructed in-house utilizing a MKS PPT electron-ionization quadrupole mass-spectrometer (MS) equipped with a heated capillary inlet (115 °C), a Lindberg tube furnace with programmable temperature control and a Brooks 5850 E-series mass flow controller. Hydrogen desorption kinetics were also characterized using a water displacement desorption (WDD) apparatus constructed in-house where the amount of desorbed gas was directly monitored from the volume of expelled water. Hydrogen desorption kinetics, reversibility, and cycling characteristics were collected using a PCT Pro-2000 Sieverts' type Pressure–Composition–Temperature (PCT) apparatus from Hy-Energy.

Phase identity and purity were characterized by XRD and FT-IR. Powder XRD (PXRD) data were collected on a SCINTAG (XDS 2) powder diffractometer operated at 45 kV and 40 mA with step increments of 0.02° measured during 0.5 s with Cu Kα radiation (λ = 1.5418 Å). All samples were maintained under an argon atmosphere during data collection using a custom-made aluminum sample holder with a Kapton® film cover and a depressed button-style sample pan. Samples were mounted into the sample pan, covered with a Parafilm® sheet, and sealed into the Al sample holder. Five peaks resulting from Parafilm® ($2\theta = 21°$ and 24°) and aluminum ($2\theta = 38°$, 45° and 65°) were manually excluded from the raw PXRD data files. High-temperature X-ray diffraction data were collected using a Bueler HDK 2.4 furnace chamber attached to a Scintag X1 diffractometer, an Inel CPS 120 position sensitive detector and collimated Cu Kα radiation. Data were collected under an atmosphere of flowing purified nitrogen (200 sccm) while the temperature was ramped at a constant rate of 2 °C/min from 50 to 450 °C following an initial room temperature scan. Scans were integrated for 5 min, each corresponding to a temperature average over a 10 °C window while ramping. Photo-acoustic infrared spectra were obtained on a Mattson Instruments Cygnus 100 FT-IR spectrometer, using an interferometer mirror velocity of 0.08 cm/s. The spectrometer was equipped with a water-cooled source. An METC Model 200 photoacoustic cell purged with helium was used through out. Sixty-five scans were averaged for sample and background data. Spectra were transformed at 8 cm^{-1} resolution with one order of zero filling. Nitrogen boil-off was used to purge the instrument and sample handling was achieved in this atmosphere by the use of a glove bag attached to the access door of the sample chamber. Samples were transferred from the preparative chamber to the spectrometer glove bag in sealed containers.

3. Results and discussion

3.1. Hydrogen desorption

Fig. 1 shows the TPD-MS analysis of the gas evolved from as-milled $2LiNH_2 + LiBH_4 + MgH_2$ sample while ramping the temperature at a rate of 5 °C/min under 100 sccm Ar flow. We note that hydrogen desorption from this ternary mixture starts at approximately 110 °C, and consists of at least four distinguishable reactions, with TPD-MS peaks at 180, 190 (shoulder), 310, and 560 °C. We also note that the amount of NH_3 release is extremely small when compared to the amount of hydrogen released.

Fig. 2 shows the constant temperature desorption kinetics at 260 and 320 °C to a 1 bar hydrogen atmosphere. The total capacity of hydrogen release is quite large, with 8.2 wt% hydrogen desorbed through three hydrogen releasing reaction steps seen in Fig. 1. The first 3.5 wt% hydrogen is released very quickly, within minutes at both temperatures. However, the remaining 4.7 wt% requires 12 h to desorb at 260 °C, a temperature below the second peak in Fig. 1, but only one hour at 320 °C, a temperature above the second peak. At either temperature, the total amount of hydrogen released is the same (8.2 wt%), implying that the temperature of the second desorption peak in Fig. 1 is kinetically limited, rather than a thermodynamic transition temperature.

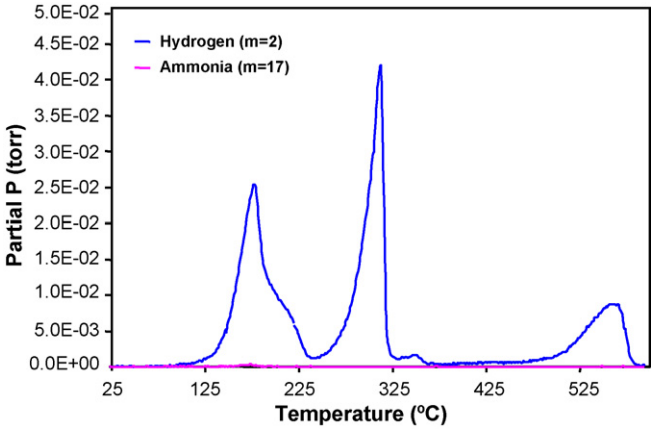

Fig. 1. TPD-MS data for the ternary composition depicting hydrogen ($m/e = 2$, blue) and ammonia ($m/e = 17$, pink) as function of temperature (5 °C/min heating rate to 575 °C).

3.2. Phase analysis

The data in Figs. 1 and 2 strongly suggest that there are multiple desorption reactions occurring in this system. To identify these reactions we have undertaken an extensive analysis of this composition as a function of temperature, using a combination of PXRD, photoacoustic detection FT-IR, and *in situ* high-temperature PXRD. Figs. 3 and 4 show respective PXRD patterns and IR spectra of the as-milled sample as well as samples that were heated (5 °C/min) and quenched at 140, 180, and 255 °C corresponding to 0.2, 2.0, and 4.0 wt% hydrogen desorbed. In the milled sample, the starting components MgH_2 and $LiBH_4$ were still visible, while $LiNH_2$ was consumed. Additionally, new phases $Li_4BH_4(NH_2)_3$ [6] and $Mg(NH_2)_2$ were formed in the milling process. Upon heating to 140 °C, but before any appreciable amount of hydrogen was released (140 °C, 0.2 wt%

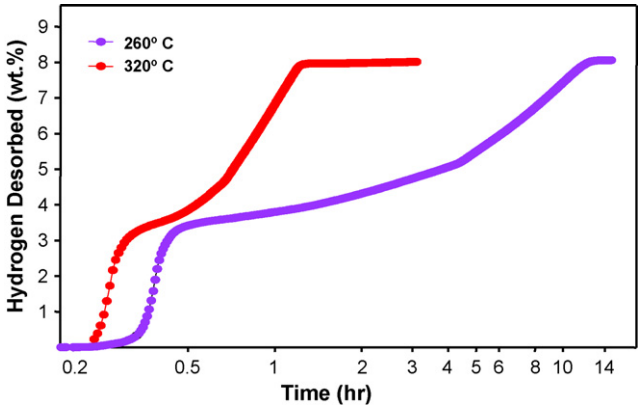

Fig. 2. Isothermal kinetic hydrogen desorption data for the ternary composition at 260 °C (purple) and 320 °C (red) vs. time (log scale). Data collected on a Sievert's type PCT apparatus.

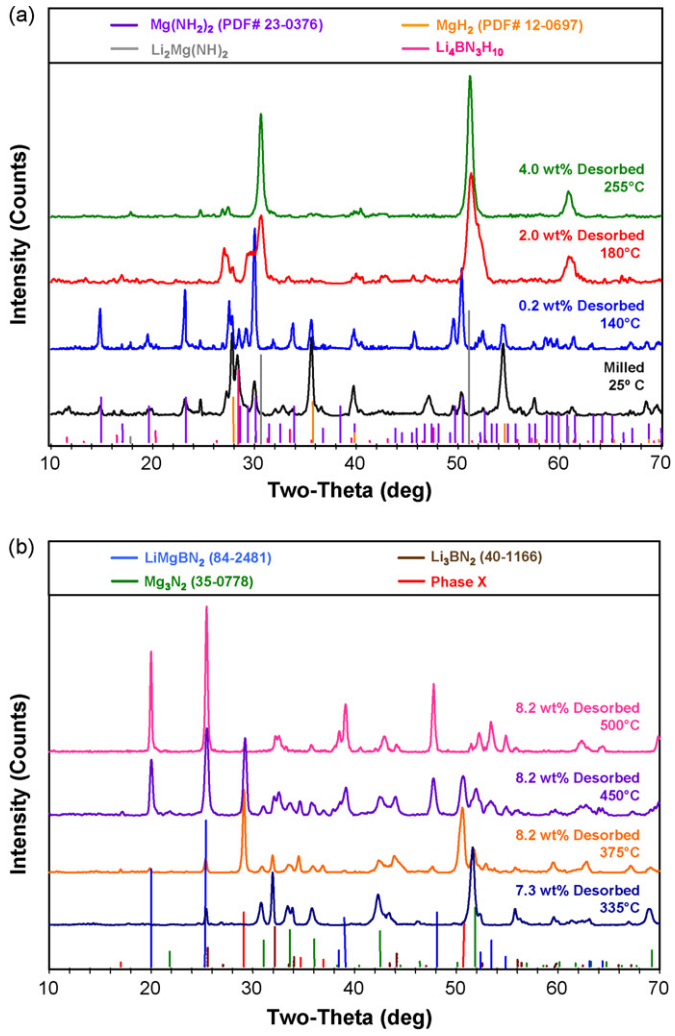

Fig. 3. PXRD patterns of: (a) as-milled sample, quenched after ramping to 140 °C (0.2 wt% H_2 desorbed), 180 °C (2.0 wt% H_2 desorbed) and 255 °C (4.0 wt% H_2 desorbed) and (b) to 335 °C (7.3 wt% H_2 desorbed), 375 °C (8.2 wt% H_2 desorbed), 450 °C (8.2 wt% H_2 desorbed), and 500 °C (8.2 wt% H_2 desorbed).

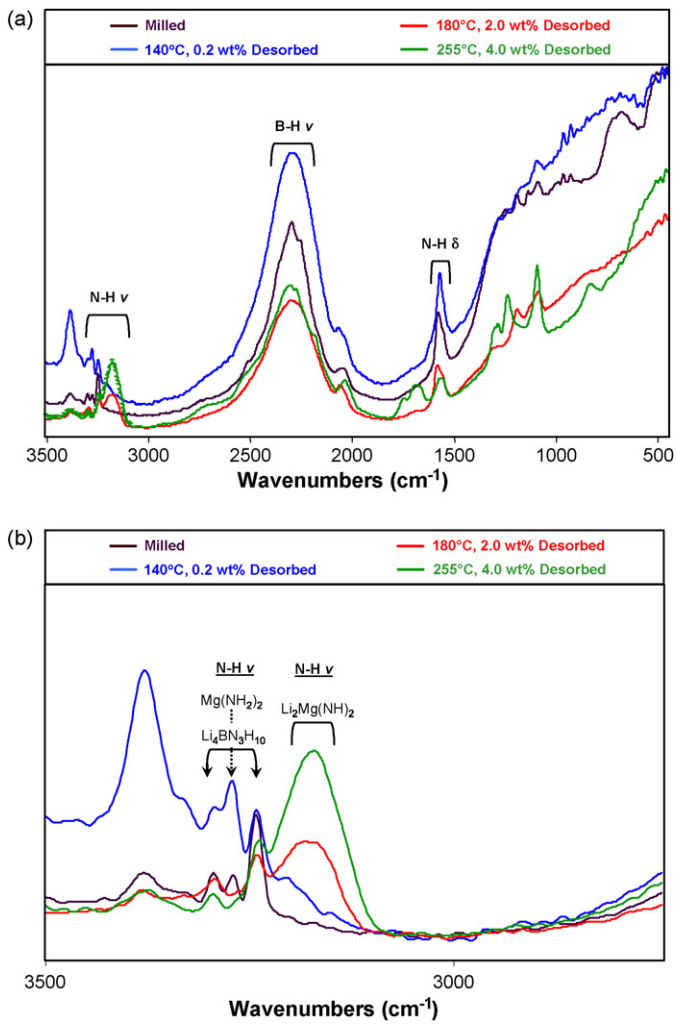

Fig. 4. FT-IR results of: (a) as-milled sample, quenched after ramping to 140 °C (0.2 wt% H_2 desorbed), 180 °C (2.0 wt% H_2 desorbed), and 255 °C (4.0 wt% H_2 desorbed) and (b) enlarged portion for wave numbers between 3500 and 2500 cm^{-1}.

desorbed), we observed a significant increase in the amount of $Mg(NH_2)_2$ and the melting of $Li_4BH_4(NH_2)_3$. The latter is indicated by the disappearance of $Li_4BH_4(NH_2)_3$ in the PXRD data, coupled with the persistence of the characteristic symmetric and asymmetric N–H (amide) stretches in IR data (3301 and 3242 cm^{-1} observed in our experiments, compared with 3303 and 3243 cm^{-1} for $Li_4BN_3H_{10}$ given in reference [6]). Further heating to 180 °C results in release of 2.0 wt% hydrogen and the formation of the mixed-imide phase, $Li_2Mg(NH)_2$. It should be noted that the phase assignment of this mixed imide is based on its three characteristic peaks at 30.7°, 51.3°, and 60.9° in PXRD data [4] as well as the signature N–H stretch in the IR data (3178 cm^{-1} observed in the present work, 3187 cm^{-1} given in [7]). As observed by both PXRD and IR, this phase continues to grow in intensity until 255 °C (4.0 wt% H_2 desorbed), which corresponds to the first peak and shoulder described in Fig. 1. Concurrently (from 140 to 255 °C or 0.2–4.0 wt%), MgH_2 and $Mg(NH_2)_2$ are completely consumed while $Li_4BH_4(NH_2)_3$ is significantly depleted. The second major hydrogen releasing event occurs between 255 and 375 °C and corresponds to a total of 4.2 wt% extra hydrogen desorbed. In this temperature region, $Li_2Mg(NH)_2$ and $LiBH_4$ are consumed and Mg_3N_2 and Li_3BN_2 are formed. From PXRD, trace amounts of LiH and an unknown phase (denoted as 'Phase X') are also detected. Subsequent heating up to 500 °C does not result in additional hydrogen release but does lead to a phase transformation consistent with the consumption of Li_3BN_2, Mg_3N_2, and $LiBH_4$ and the production of LiH and $LiMgBN_2$, a phase which was reported in the literature to form only under high temperature conditions (1477 °C from Li_3N, Mg_3N_2, and BN) [8]. The final hydrogen releasing step (>500 °C) is attributed to decomposition of LiH (third peak in Fig. 1).

Fig. 5 shows a contour plot of the results from an *in situ* high temperature PXRD measurement. This *in situ* experiment confirms the phase formation sequence as observed from Figs. 3 and 4 described above, but also reveals additional quantitative information in terms of the phase transformation temperatures. Specifically, during the initial heating of the

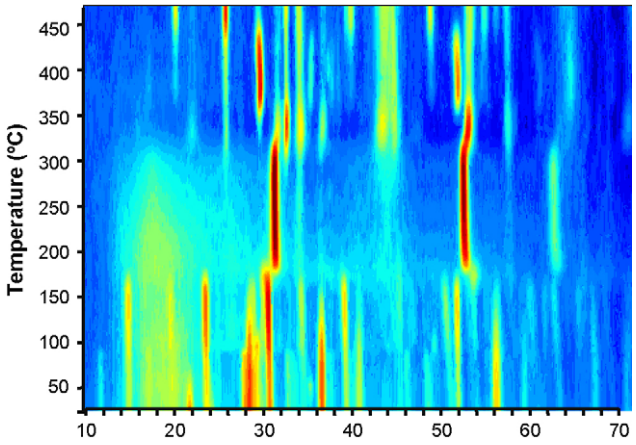

Fig. 5. Contour plot of *in situ* XRD for the ternary composition as a function of temperature (25–450 °C).

milled sample it is evident that prior to any hydrogen release, $Li_4BH_4(NH_2)_3$ and MgH_2 phases rapidly disappear by 100 and 150 °C, respectively. The melting of $Li_4BH_4(NH_2)_3$ occurs at a lower temperature than previously observed (150 °C) [9], an interesting point which may play an important role in improving the kinetics of the reversible reaction in this ternary system. Based on the combination of above phase analysis results, we arrive at the following reactions for the first peak, shoulder, and second peak reactions of Fig. 1, respectively:

$$2Li_4BH_4(NH_2)_3 + 3MgH_2 \Rightarrow 3Li_2Mg(NH)_2 + 2LiBH_4 + 6H_2 \text{ (first peak)} \quad (2)$$

$$Mg(NH_2)_2 + 2LiH \Rightarrow Li_2Mg(NH)_2 + 2H_2 \text{ (shoulder)} \quad (3)$$

$$3Li_2Mg(NH)_2 + 2LiBH_4 \Rightarrow 2Li_3BN_2 + Mg_3N_2 + 2LiH + 6H_2 \text{ (second peak)} \quad (4)$$

To the best of our knowledge, this is the first observation of the *new* desorption reactions (2) and (4). Reaction (3) is the previously discovered [4,5] reversible reaction (1). We note that both first peak and shoulder reactions form the mixed imide phase $Li_2Mg(NH)_2$, which is subsequently consumed in the second peak hydrogen desorption to form nitride phases and LiH.

3.3. Reversibility

Fig. 6(a) shows the desorption kinetics over five cycles of the as-prepared and recharged sample at 180 °C to 1 bar hydrogen atmosphere. The as-milled sample desorbed approximately 3.0 wt% hydrogen within 10 min. After recharging at 180 °C and 100 bar hydrogen, it then reversibly releases 2.8 wt% hydrogen in the next four cycles. TPD-MS of the as-prepared and recharged samples are compared in Fig. 6(b). The first peak shifts to a higher temperature upon recharge, overlapping the shoulder region in the milled sample. We thus conclude that the "shoulder" reaction (reaction (3), above) is the reversible reaction in our material. Especially noteworthy from Fig. 6 is the significantly improved kinetics of the ternary mixture at 180 °C,

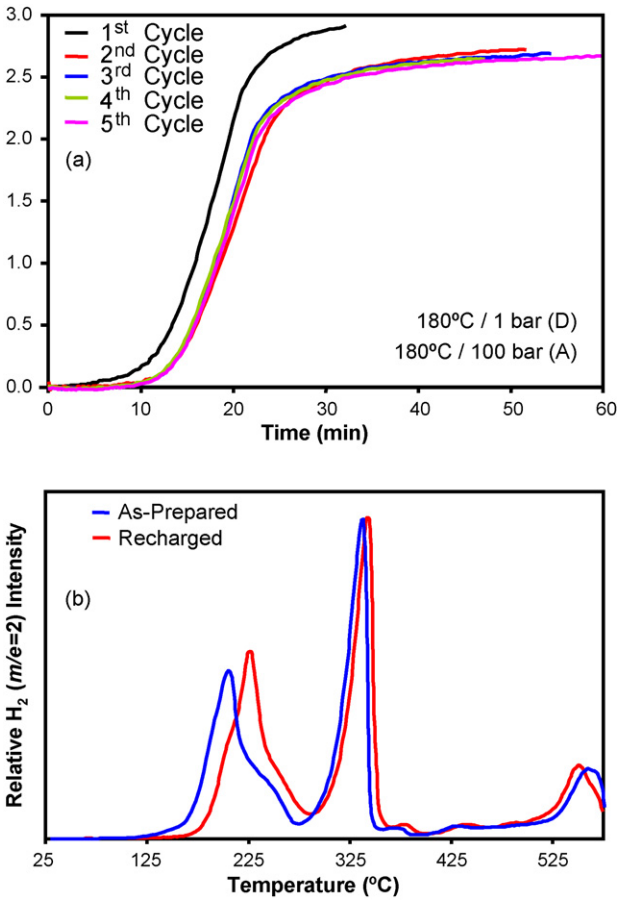

Fig. 6. (a) Hydrogen desorption kinetics at 180 °C and 1 bar over five cycles after subsequent charging (180 °C and 100 bar hydrogen). (b) Hydrogen desorption TPD-MS curves (5 °C/min heating rate to 575 °C) for the as-prepared sample (blue) and recharged sample (red) illustrating shift in reaction event contributions.

as compared to the reaction kinetics obtained from the binary combination of $LiNH_2$ and MgH_2 [10,11]

3.4. Discussion

The reversible reaction (3) between $Li_2Mg(NH)_2$ and $2LiH + Mg(NH_2)_2$ has a theoretical capacity of 5.6 wt% hydrogen and from its measured thermodynamics [5], it is predicted to desorb to 1 bar pressure at 90 °C. However, when this reaction is initiated from a binary mixture of $2LiNH_2 + MgH_2$, temperatures of 220 °C or more are required to achieve reasonable kinetics, and a small amount of NH_3 accompanies H_2 desorption.

Given these limitations of the binary mixture, it is quite intriguing that our ternary mixture $2LiNH_2$–$LiBH_4$–MgH_2 gives the same reversible reaction but with substantially improved kinetics and suppressed NH_3 release. We suggest that the improved kinetics are due to a unique "self-catalyzing" process present in the ternary mixture. The solid-state product of reaction (3), $Li_2Mg(NH)_2$, is also produced by reaction (2), which precedes reaction (3) in temperature. We propose that the generation of $Li_2Mg(NH)_2$ in reaction (2) effectively "seeds" or acts as nucleation agent for reaction (3), reducing its temperature and increasing its reaction rate [11].

More specifically, the $Li_4BH_4(NH_2)_3$ phase formed during milling further reacts with MgH_2 to form $Mg(NH_2)_2$. The $Mg(NH_2)_2$ phase continues to grow upon further heating, partially consuming $Li_4BH_4(NH_2)_3$ and MgH_2. At approximately 100 °C, $Li_4BH_4(NH_2)_3$ melts and $Li_2Mg(NH)_2$ precipitates via reaction (2) between the remaining molten $Li_4BH_4(NH_2)_3$ and MgH_2. These precipitated $Li_2Mg(NH)_2$ particles may act as seeds for further formation of $Li_2Mg(NH)_2$ from $Mg(NH_2)_2$ and LiH formed during ball milling and upon heating. This reaction scheme improves the low temperature kinetics by supplying nuclei and controlling the grain size of the mixed imide phase. It also suppresses the formation of NH_3 due to the low desorption/recharging temperature. $LiBH_4$ and LiH phases could inhibit grain growth in the cycling process and provide hydrogen diffusion pathways. The negligible loss of N from NH_3 release also improves the cycling performance of the reversible reactions.

4. Conclusions

Via an in-depth exploration of the ternary mixture, $2LiNH_2$–$LiBH_4$–MgH_2, we have identified several novel hydrogen storage reactions, and improved kinetic response in a known reaction. We find a self-catalyzing reaction which improves the low temperature kinetics of the reversible reaction between $Li_2Mg(NH)_2$ and $2LiH + Mg(NH_2)_2$. During low-temperature desorption, the reaction between molten $Li_4BH_4(NH_2)_3$ and MgH_2 forms dispersed $Li_2Mg(NH)_2$ "seeds", which serve to accelerate the reversible reaction, providing significant desorption at lower temperatures than previously observed. Additionally, the formation of NH_3 from amide decomposition is significantly suppressed in the ternary mixture, translating to improved low temperature cycling behavior.

References

[1] B. Bogdanović, M. Schwickardi, J. Alloys Compd. 253–254 (1997) 1.
[2] P. Chen, Z. Xiong, J. Luo, J. Lin, K. Tan, Nature 420 (2002) 302.
[3] F.E. Pinkerton, G. Meisner, M. Meyer, M. Balogh, M. Kundrat, J. Phys. Chem. 109B (2005) 6.
[4] Z. Xiong, G. Xiong, J. Wu, P. Hu, Chen, Adv. Mater. 16 (2004) 1522.
[5] W. Luo, J. Alloys Compd. 381 (2004) (2004) 316, 284, 385.
[6] P.A. Chater, W.I.F. David, S.R. Johnson, P.P. Edwards, P.A. Anderson, Chem. Commun. 23 (2006) 2439.
[7] P. Chen, Z. Xiong, L. Yang, G. Wu, W. Luo, J. Phys. Chem. 110B (2006) 14221.
[8] U. Herterich, J. Curda, K. Peters, M. Somer, H.G. von Schnering, Zeitschrift für Kristallographie 209 (1994) 617.
[9] G. Meisner, M. Scullin, M. Balogh, F. Pinkerton, M. Meyer, J. Phys. Chem. 110B (2006) 4186.
[10] J. Yang, A. Sudik, C. Wolverton, J. Alloys Compd. 430 (2007) 334.
[11] A. Sudik, J. Yang, D. Halliday, C. Wolverton, J. Phys. Chem. C 111 (2007) 6568–6573.